PHYSICAL REVIEW B **94**, 214516 (2016)

Spin anisotropy due to spin-orbit coupling in optimally hole-doped $Ba_{0.67}K_{0.33}Fe_2As_2$

Yu Song,[1,*] Haoran Man,[1] Rui Zhang,[1] Xingye Lu,[1] Chenglin Zhang,[1] Meng Wang,[2] Guotai Tan,[3] L.-P. Regnault,[4,5] Yixi Su,[6] Jian Kang,[7] Rafael M. Fernandes,[7] and Pengcheng Dai[1,3,†]

[1]*Department of Physics and Astronomy, Rice University, Houston, Texas 77005, USA*
[2]*Department of Physics, University of California, Berkeley, California 94720, USA*
[3]*Center for Advanced Quantum Studies and Department of Physics, Beijing Normal University, Beijing 100875, China*
[4]*Université Grenoble Alpes, 38042 Grenoble, France*
[5]*CEA-Grenoble, INAC-MEM-MDN, 38054 Grenoble, France*
[6]*Jülich Centre for Neutron Science, Forschungszentrum Jülich GmbH, Outstation at MLZ, D-85747 Garching, Germany*
[7]*School of Physics and Astronomy, University of Minnesota, Minneapolis, Minnesota 55455, USA*

(Received 17 September 2016; revised manuscript received 29 November 2016; published 23 December 2016)

We use polarized inelastic neutron scattering to study the temperature and energy dependence of spin space anisotropies in the optimally-hole-doped iron pnictide $Ba_{0.67}K_{0.33}Fe_2As_2$ ($T_c = 38$ K). In the superconducting state, while the high-energy part of the magnetic spectrum is nearly isotropic, the low-energy part displays a pronounced anisotropy, manifested by a c-axis polarized resonance. We also observe that the spin anisotropy in superconducting $Ba_{0.67}K_{0.33}Fe_2As_2$ extends to higher energies compared with electron-doped $BaFe_{2-x}TM_xAs_2$ (TM = Co, Ni) and isovalent-doped $BaFe_2As_{1.4}P_{0.6}$, suggesting a connection between T_c and the energy scale of the spin anisotropy. In the normal state, the low-energy spin anisotropy for hole- and electron-doped iron pnictides near optimal superconductivity onset at temperatures similar to the temperatures at which the elastoresistance deviates from Curie–Weiss behavior, pointing to a possible connection between the two phenomena. Our results highlight the relevance of the spin-orbit coupling to the superconductivity of the iron pnictides.

DOI: 10.1103/PhysRevB.94.214516

I. INTRODUCTION

The parent compounds of iron pnictide superconductors, such as LaFeAsO and $BaFe_2As_2$, form stripe antiferromagnetic (AF) order at T_N below a tetragonal-to-orthorhombic structural transition temperature T_S [inset in Fig. 1(b)] [1–4]. Superconductivity can be induced by partially replacing Ba by K in $BaFe_2As_2$ to form hole-doped $Ba_{1-x}K_xFe_2As_2$ [5–9] or by partially replacing Fe by TM (TM = Co, Ni) to form electron-doped $BaFe_{2-x}TM_xAs_2$ [10–13]. Importantly, the resulting phase diagrams exhibit significant asymmetry between electron- and hole-doping [Figs. 1(a) and 1(b)] [3,4]. For instance, while near optimal doping the stripe AF order becomes incommensurate for electron-doped $BaFe_{2-x}TM_xAs_2$ [12,13] [see arrow in Fig. 1(b)], a double-**Q** tetragonal magnetic structure with ordered moments along the c axis is observed in hole-doped $Ba_{1-x}K_xFe_2As_2$ [see region of the phase diagram near the arrow and inset in Fig. 1(a)] [6–9].

Nevertheless, upon entering the superconducting state, a magnetic resonance mode appears in the magnetic spectrum in both cases at the AF wave vector ($\mathbf{Q}_{AF}$) [14–17]. Furthermore, by measuring the splitting of the electronic states at high-symmetry points in reciprocal space [18], angle-resolved photoemission spectroscopy (ARPES) measurements find that spin-orbit coupling (SOC) is present in both electron- and hole-doped iron pnictides with a similar energy scale ~10 meV [19]. Also common to both optimally-electron-doped $BaFe_{2-x}TM_xAs_2$ [20,21] and -hole-doped $Ba_{1-x}K_xFe_2As_2$ [22,23] is the presence of electronic nematic fluctuations, as revealed by the elastoresistance, i.e., the rate of change of the resistivity anisotropy with respect to applied in-plane uniaxial strain [Fig. 1(c)] [24]. The elastoresistance diverges with a Curie–Weiss form for both classes of materials as well as for isovalent-doped $BaFe_2As_{1.4}P_{0.6}$ [25]. Deviation from the Curie–Weiss behavior is seen in both optimally-electron- and -hole-doped $BaFe_2As_2$ at low temperatures, while no deviation is seen in $BaFe_2As_{1.4}P_{0.6}$ down to T_c [Fig. 1(d)] [25].

In addition to its impact on the electronic spectrum [19,26], SOC also converts crystalline anisotropies into anisotropies in spin space, as seen from nuclear magnetic resonance studies [27]. The spin anisotropy resulting from SOC plays an essential role for the double-**Q** magnetic phase [6–9], in which the ordered moments align along the c axis [28]. If SOC was absent, the spin excitations in the paramagnetic tetragonal state of the iron pnictides would be isotropic in spin space [Fig. 1(e)]. However, due to the presence of a sizable SOC, an anisotropy is developed in the spin excitations, which can be quantitatively determined by neutron polarization analysis [29]. In the antiferromagnetically ordered phases of the parent compounds $BaFe_2As_2$ and NaFeAs [30,31], where the ordered moments point parallel to the orthorhombic a axis [inset in Fig. 1(b)], spin waves exhibit significant anisotropy, with c-axis polarized spin waves occurring at lower energy compared with b-axis polarized spin waves [32–34]. To elucidate the relevance of SOC to superconductivity, it is instructive to compare the behavior of the spin anisotropy in hole-doped and electron-doped $BaFe_2As_2$, since the maximum values of T_c are quite different in these two cases—$T_c \approx 38$ K for optimally-hole-doped $Ba_{0.67}K_{0.33}Fe_2As_2$ and $T_c \approx 25$ K for optimally-electron-doped $BaFe_{1.86}Co_{0.14}As_2$. Previous analysis of the electron-doped case revealed that the spin anisotropy persists in the paramagnetic tetragonal phase for doping levels up to or slightly beyond optimal

*Yu.Song@rice.edu
†pdai@rice.edu

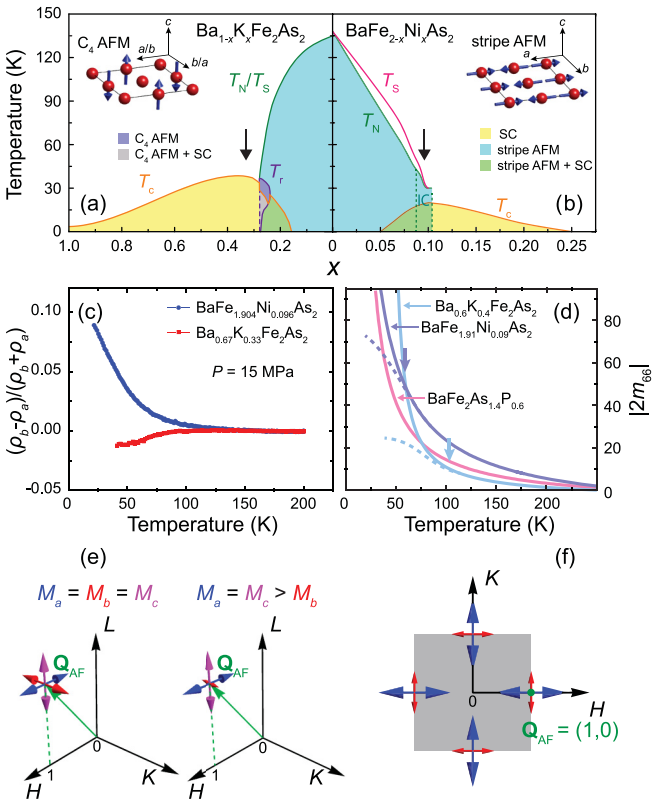

FIG. 1. The electronic phase diagrams of (a) hole- and (b) electron-doped $BaFe_2As_2$. While parent compounds of iron pnictides have stripe AF order [inset in panel (b)] [2], the tetragonal double-**Q** C_4 AF order is found in hole-doped $BaFe_2As_2$ near optimal superconductivity [inset in panel (a)] [6–9]. T_S, T_N, T_c, and T_r mark the tetragonal-to-orthorhombic structural transition, the paramagnetic-to-AF transition, the superconducting transition, and the transition into the C_4 magnetic phase. The phase diagrams in panels (a) and (b) are adapted from Refs. [43] and [4]. (c) Resistivity anisotropy $(\rho_a - \rho_b)/(\rho_a + \rho_b)$ of $BaFe_{1.904}Ni_{0.096}As_2$ and $Ba_{0.67}K_{0.33}Fe_2As_2$ under uniaxial pressure of $P = 15$ MPa measured by using a mechanical clamp that can vary applied pressure *in situ* [44,45]. (d) Elastoresistance $|2m_{66}|$ for optimally doped $BaFe_{1.91}Ni_{0.09}As_2$, $Ba_{0.6}K_{0.4}Fe_2As_2$, and $BaFe_2As_{1.4}P_{0.6}$, adapted from Ref. [25]. The solid lines are Curie–Weiss fits to the data and the dashed lines represent deviations from the Curie–Weiss form. Vertical arrows mark the temperature at which such deviations begin. (e) Schematic of isotropic spin excitations (left) and anisotropic spin excitations (right), with the sizes of arrows centered at $\mathbf{Q}_{AF}$ representing the intensities of spin excitations polarized along different directions. (f) In-plane spin anisotropy discussed in this work (represented by red and blue arrows of different sizes) preserves four-fold rotational symmetry of the tetragonal unit cell because $\mathbf{Q}_{AF}$ is at an edge of the Brillouin zone of the unfolded tetragonal (i.e., 1-Fe) unit cell [46], depicted by the shaded gray area.

doping [35–40] but vanishes in the well-overdoped regime [40,41].

In this paper, we present polarized neutron scattering studies of spin excitations in optimally hole-doped $Ba_{0.67}K_{0.33}Fe_2As_2$ [15,38]. In the normal state, we find that the spin anisotropy of $Ba_{0.67}K_{0.33}Fe_2As_2$ persists to ∼100 K for $E = 3$ meV, similarly to the case of near-optimally electron-doped $BaFe_{2-x}TM_xAs_2$, where spin anisotropy at $\mathbf{Q}_{AF} = (1,0,1)$ was found below $E \approx 7$ meV and up to ∼70 K [36,37]. We associate the onset of normal-state spin anisotropy with the nematic susceptibility deviating from Curie–Weiss behavior measured via elastoresistance [see vertical arrows in Fig. 1(d)] [25], indicating an important role of spin excitations in transport properties of iron pnictides.

Upon entering the superconducting state, we find that, while at high energies ($E \geqslant 14$ meV), the spectrum is nearly isotropic as found in previous work [38], at low energies the resonance mode is strongly anisotropic, being dominated by a c-axis polarized component. We attribute this behavior to the fact that the superconducting state is close to the double-**Q** magnetic phase, in which the magnetic moments point out of plane [7,8]. Indeed, by adding a spin-anisotropic term that favors c-axis spin orientation in a simple two-band theoretical model, we find that the resonance mode in the c-axis polarized channel has in general a lower energy than in other channels, and that this energy difference increases as the magnetically ordered state is approached. Our analysis also reveals an interesting correlation between the energy scale of the spin anisotropy in the superconducting state and T_c [35–40,42], suggesting that SOC is an integral part of the superconductivity of iron pnictides.

II. EXPERIMENTAL RESULTS

Polarized inelastic neutron-scattering measurements were carried out by using the IN22 triple-axis spectrometer at Institut Laue–Langevin in Grenoble, France. We studied $Ba_{0.67}K_{0.33}Fe_2As_2$ single crystals ($a = b \approx 5.56$ Å, $c = 13.29$ Å) co-aligned in the $[H,0,L]$ scattering plane used in previous works [38,47]. We use the orthorhombic notation suitable for AF-ordered iron pnictides even though $Ba_{0.67}K_{0.33}Fe_2As_2$ has a tetragonal structure and is paramagnetic at all temperatures [15,38]. Thus, the momentum transfer is $\mathbf{Q} = H\mathbf{a}^* + K\mathbf{b}^* + L\mathbf{c}^*$, with $\mathbf{a}^* = \frac{2\pi}{a}\hat{\mathbf{a}}$, $\mathbf{b}^* = \frac{2\pi}{b}\hat{\mathbf{b}}$, and $\mathbf{c}^* = \frac{2\pi}{c}\hat{\mathbf{c}}$, where H, K, and L are Miller indices. In this notation, magnetic order in $BaFe_2As_2$ occurs at $\mathbf{Q}_{AF} = (1,0,L)$ with $L = 1,3,5,\ldots$ [Fig. 1(e)]. Three neutron spin-flip (SF) cross sections σ_x^{SF}, σ_y^{SF}, and σ_z^{SF} were measured, with the usual convention $x \parallel \mathbf{Q}$, $y \perp \mathbf{Q}$ and in the scattering plane, and z perpendicular to the scattering plane. Magnetic neutron scattering directly measures the magnetic scattering function $S^{\alpha\beta}(\mathbf{Q},E)$, which is proportional to the imaginary part of the dynamic susceptibility through the Bose factor, $S^{\alpha\beta}(\mathbf{Q},E) \propto [1 - \exp(-\frac{E}{k_BT})]^{-1}\mathrm{Im}\chi^{\alpha\beta}(\mathbf{Q},E)$ [48]. Following earlier works [34,36,38,40,41], we denote the diagonal components of the magnetic scattering function $S^{\alpha\alpha}$ as M_α. M_y and M_z can be obtained from measured SF cross sections through $\sigma_x^{SF} - \sigma_y^{SF} \propto M_y$ and $\sigma_x^{SF} - \sigma_z^{SF} \propto M_z$. M_y and M_z are related to $M_a = M_{100}$, $M_b = M_{010}$, and $M_c = M_{001}$ through $M_y = \sin^2\theta M_a + \cos^2\theta M_c$ and $M_z = M_b$ [34,36,38,40,41], with θ being the angle between $\mathbf{Q}$ and $\mathbf{a}^*/\mathbf{a}$. Anisotropy between M_a and M_b at $\mathbf{Q}_{AF}$ is allowed in the paramagnetic tetragonal state of iron pnictides and does not break four-fold rotation symmetry of the lattice because $\mathbf{Q}_{AF}$ is at an edge of the Brillouin zone of the unfolded tetragonal (1-Fe) unit cell [46], as depicted in Fig. 1(f). Another manifestation of the lack of four-fold rotational symmetry for magnetic excitations

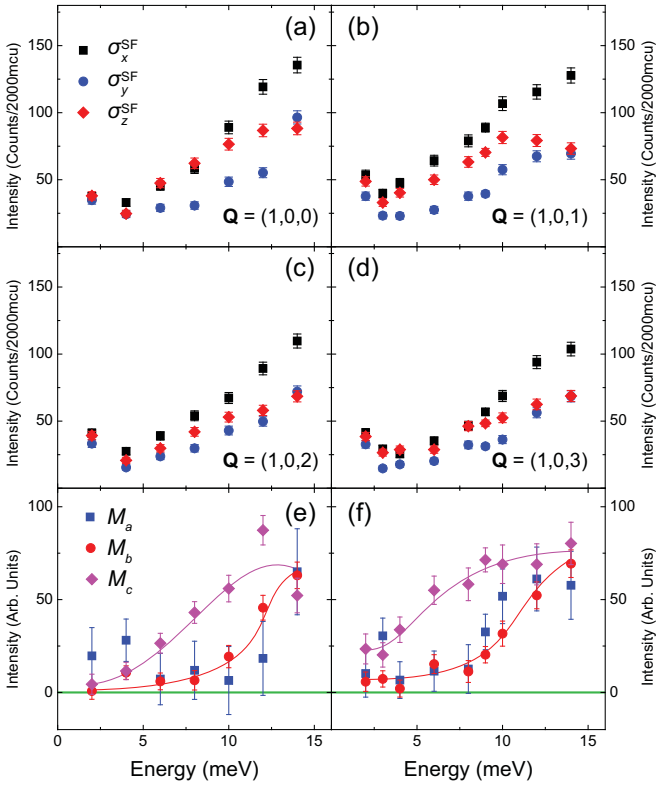

FIG. 2. Constant-**Q** scans of $\sigma_x^{\rm SF}$, $\sigma_y^{\rm SF}$, and $\sigma_z^{\rm SF}$ at $\mathbf{Q} = (1,0,L)$ for (a) $L = 0$, (b) $L = 1$, (c) $L = 2$, and (d) $L = 3$ measured at 2 K. By using the measured cross sections in panels (a)–(d), M_a, M_b, and M_c are obtained for (e) even and (f) odd L. The solid lines are to guide the eye.

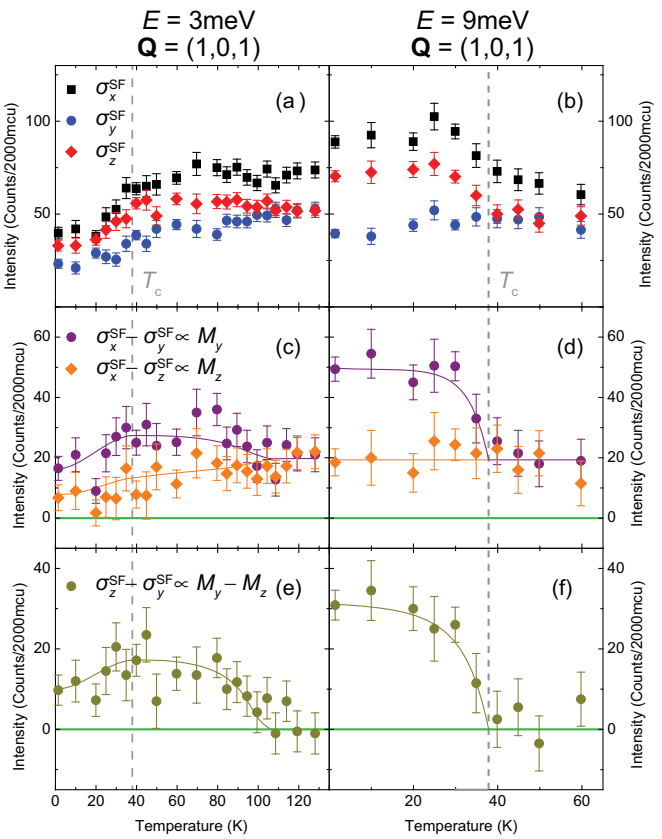

FIG. 3. Temperature scans of $\sigma_x^{\rm SF}$, $\sigma_y^{\rm SF}$, and $\sigma_z^{\rm SF}$ at $\mathbf{Q} = (1,0,1)$ with (a) $E = 3$ meV and (b) $E = 9$ meV. The differences $\sigma_x^{\rm SF} - \sigma_y^{\rm SF}$ and $\sigma_x^{\rm SF} - \sigma_z^{\rm SF}$ which are respectively proportional to M_y and M_z are shown for (c) $E = 3$ meV and (d) $E = 9$ meV. The differences $\sigma_z^{\rm SF} - \sigma_y^{\rm SF}$ which is proportional to $M_y - M_z$ are shown for (e) $E = 3$ meV and (f) $E = 9$ meV. The solid lines are guides to the eye. The dashed vertical lines mark T_c.

at $\mathbf{Q}_{\rm AF}$ is the anisotropic in-plane correlation lengths seen in the paramagnetic tetragonal states of $BaFe_2As_2$ [49] and $CaFe_2As_2$ [50]. By obtaining M_y and M_z at two equivalent wave vectors with different θ, it is then possible to obtain M_a, M_b, and M_c [33,34,36,40].

Figure 2 summarizes constant-**Q** scans at 2 K and $\mathbf{Q} = (1,0,L)$ with $L = 0, 1, 2$, and 3. From Figs. 2(a)–2(d), it is clear that $\sigma_x^{\rm SF} > \sigma_z^{\rm SF} \geqslant \sigma_y^{\rm SF}$ below $E \approx 14$ meV, meaning that spin anisotropy exists below this energy while excitations above this energy are isotropic as shown in previous work [38]. Although magnetic order is fully suppressed in $Ba_{0.67}K_{0.33}Fe_2As_2$, the spin gap E_g in the superconducting state displays strong L dependence, with $E_g \approx 0.75$ meV for odd L and $E_g \approx 5$ meV for even L [15,38]. From Figs. 2(b) and 2(d), we observe that the small gap for odd L is due to M_y, with $\sigma_x^{\rm SF} \approx \sigma_z^{\rm SF} > \sigma_y^{\rm SF}$ for $E \lesssim 5$ meV. Magnetic excitations are gapped in the same energy range for even L, as can be seen in Figs. 2(a) and 2(c), with $\sigma_x^{\rm SF} \approx \sigma_y^{\rm SF} \approx \sigma_z^{\rm SF}$. M_a, M_b, and M_c for even and odd L are shown in Figs. 2(e) and 2(f), respectively. While M_b is weakly L dependent, M_c clearly displays different behavior for even and odd L. Because, in the energy range $5 \lesssim E \lesssim 10$ meV, M_c dominates and is dispersive along L, we uniquely identify it with the the anisotropic resonance that disperses along L which was previously observed in the same sample [38].

To gain further insight into the spin anisotropy of $Ba_{0.67}K_{0.33}Fe_2As_2$, we carried out temperature scans at $\mathbf{Q}_{\rm AF} = (1,0,1)$ for $E = 3$ meV and $E = 9$ meV, as shown in Figs. 3(a) and 3(b). At $E = 3$ meV, the spin anisotropy with $\sigma_z^{\rm SF} > \sigma_y^{\rm SF}$ persists up to ~100 K. Although below T_c the magnetic signal is suppressed in all three SF cross sections, the normal-state anisotropy persists [Fig. 3(a)]. At $E = 9$ meV, the spin anisotropy disappears above T_c, suggesting that the main contribution to the spin anisotropy in the superconducting state arises from the anisotropic resonance mode [38]. In Figs. 3(c) and 3(d), $\sigma_x^{\rm SF} - \sigma_y^{\rm SF} \propto M_y$ and $\sigma_x^{\rm SF} - \sigma_z^{\rm SF} \propto M_z$ are shown. At $E = 3$ meV, $M_y > M_z$ for $T \lesssim 100$ K and both are suppressed below T_c. At $E = 9$ meV, while a clear resonance mode with an order-parameter-like temperature dependence is seen in M_y, M_z remains constant across T_c. The temperature onset of spin anisotropy is more clearly seen in Figs. 3(e) and 3(f), which plots $\sigma_z^{\rm SF} - \sigma_y^{\rm SF} \propto M_y - M_z$ for $E = 3$ meV and $E = 9$ meV, respectively.

To obtain the temperature dependence of M_a, M_b, and M_c, we measured $\sigma_x^{\rm SF}$, $\sigma_y^{\rm SF}$, and $\sigma_z^{\rm SF}$ at $\mathbf{Q}_{\rm AF} = (1,0,3)$ for $E = 3$ meV and $E = 9$ meV [44]. Combining the temperature dependence for $L = 1$ and $L = 3$, M_a, M_b, and M_c are obtained for odd L as shown in Figs. 4(a) and 4(b). At $E = 3$ meV, $M_a \approx M_c > M_b$ within the probed temperature range, and all three channels decrease in intensity below T_c. At $E = 9$ meV, M_a and M_b display a weak temperature

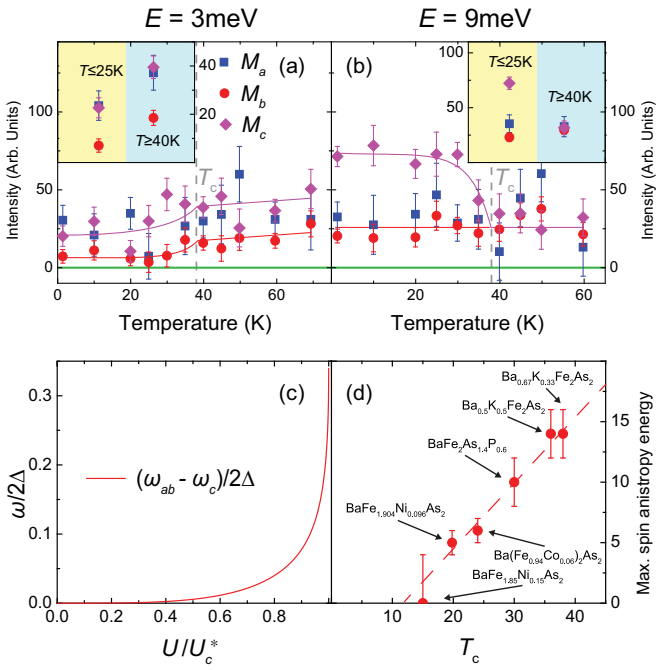

FIG. 4. Temperature dependence of M_a, M_b, and M_c for (a) $E = 3$ meV and (b) $E = 9$ meV. The solid lines are to guide the eye and dashed vertical lines mark T_c. The insets in panels (a) and (b) show binned M_a, M_b, and M_c from panels (a) and (b) for $T \leqslant 25$ K and $T \geqslant 38$ K. The insets share the same y-axis label as panels (a) and (b). (c) Difference between the energies of the ab-polarized and the c-polarized resonance modes obtained in our theoretical model. U is the electronic interaction that triggers long-range magnetic order with the moments pointing along the c axis when $U = U_c^*$ [44]. (d) Maximum energy at which spin anisotropy is observed in the superconducting state of several doped $BaFe_2As_2$ compounds. Results are obtained from Refs. [36–39,41,42]. For overdoped $BaFe_{1.85}Ni_{0.15}As_2$, the excitations are isotropic but low-energy excitations are gapped below $E \approx 4$ meV [41]; therefore, for this compound we assign the maximum spin anisotropy energy to be 0, but with an uncertainty of 4 meV.

dependence while M_c is sharply affected by T_c. To corroborate our conclusion, we binned data points in Figs. 4(a) and 4(b) that are well below T_c ($T \leqslant 25$ K) and above T_c ($T \geqslant 40$ K), as shown in the insets of Figs. 4(a) and 4(b). While magnetic excitations at $E = 3$ meV are suppressed upon entering the superconducting state, the polarization of these magnetic excitations seems to remain the same, persisting up to $T \approx 100$ K. On the other hand, at $E = 9$ meV, magnetic excitations are nearly isotropic above T_c, while $M_c > M_a \approx M_b$ well below T_c. Therefore, the c-axis polarized anisotropic resonance is directly coupled to superconductivity with an order-parameter-like temperature dependence.

III. DISCUSSION AND CONCLUSION

To understand the origin of this c-axis polarized spin resonance, we consider a simple two-band model [44] in which the resonance mode arises due to the sign change of the gap function between a hole pocket and an electron pocket displaced from each other by the AF ordering vector $\mathbf{Q}_{AF}$ [51–53]. Without SOC, the energy of the resonance mode is the same for all polarizations, being close to 2Δ far from the putative magnetic quantum phase transition inside the superconducting dome [$U \ll U_c^*$ in Fig. 4(c)], but vanishing as the transition is approached [$U \to U_c^*$ in Fig. 4(c)]. SOC, however, promotes a spin anisotropy term that makes the magnetic moments point along the c axis for hole-doped compounds [28]. As a result, the energy of the resonance mode polarized along the c axis is suppressed much faster as the magnetic transition is approached, yielding $\omega_c < \omega_{ab}$ [Fig. 4(c)]. This behavior is in qualitative agreement with our experimental results, with the resonance seen in M_c indeed at lower energies. It should also be noted that our model does not capture the broadening of the resonance, which is rather pronounced in the experimental data. Our simple model has two additional consequences: first, as the system is overdoped and moves farther from the magnetically ordered state, the resonance mode should become more isotropic. While spin anisotropy persists in slightly overdoped $Ba_{0.5}K_{0.5}Fe_2As_2$ ($T_c = 36$ K) [39], how it evolves in K-well-overdoped samples remains to be seen. Furthermore, because in electron-doped compounds the moments point along the a direction, the resonance is expected to be polarized along the a axis. Although this is the case in electron-doped $NaFe_{0.985}Co_{0.015}As$ [40], the sample studied had long-range AF order. For electron-doped $Ba(Fe_{0.94}Co_{0.06})_2As_2$ [37], the anisotropic resonance was argued to be also polarized along c axis, based on the assumption $M_a = M_b$ and the observation $M_y > M_z = 0$ for the anisotropic resonance. As we have shown here and in previous work [36], even in the tetragonal state M_a and M_b are not necessarily the same and it is unclear whether there is also significant resonance spectral weight polarized along the a axis in previous work [37]. Spin anisotropy of spin excitations has also been detected in the superconducting states of LiFeAs [54] and $FeSe_{0.5}Te_{0.5}$ [55], consistent with significant spin-orbit coupling detected by ARPES [19,26] in these systems.

The normal-state spin anisotropy at low energies persists to a temperature significantly higher than T_c [$\sim$70 K in $BaFe_{1.094}Ni_{0.096}As_2$ [36] and $\sim$100 K in $Ba_{0.67}K_{0.33}Fe_2As_2$; Fig. 3(e)] for both electron- and hole-doped $BaFe_2As_2$ near optimal doping. The temperature at which spin anisotropy onsets is similar to the temperature at which the nematic susceptibility deviates from Curie–Weiss behavior [25], suggesting a common origin for both phenomena [Fig. 1(d)]. For optimally doped $BaFe_2As_{1.4}P_{0.6}$, whose nematic susceptibility shows no deviation from the Curie–Weiss form [Fig. 1(d)] [25], no spin anisotropy is observed right above T_c [42]. While disorder is likely to play an important role in explaining this deviation from Curie–Weiss behavior in the elastoresistance [25], our results suggest that the spin anisotropy may also be important. Indeed, previous inelastic neutron scattering experiments revealed the intimate relationship between nematicity and magnetic fluctuations [56–58]. Theoretically, the nematic susceptibility increases with increasing magnetic fluctuations in all polarization channels [24]. However, once a spin anisotropy sets in, fluctuations related to the spin components perpendicular to the easy axis increase more slowly with decreasing temperature. As a result, the nematic susceptibility should also increase more slowly, which may contribute to the deviation from Curie–Weiss behavior observed experimentally.

Finally, the maximum energies at which spin anisotropy is observed in the superconducting states of several doped $BaFe_2As_2$ compounds are plotted as a function of T_c in Fig. 4(d). Note that the spin anisotropy of the resonance in the superconducting state is also present in $BaFe_2As_{1.4}P_{0.6}$, despite the absence of spin anisotropy in the normal state [42]. We note a clear positive correlation between the energy scale of the spin anisotropy and T_c, suggesting SOC to be an important ingredient for understanding superconductivity in iron pnictides.

ACKNOWLEDGMENTS

We thank Ilya Eremin, Qimiao Si, and Jiangping Hu for useful discussions. The neutron work at Rice is supported by the U.S. NSF-DMR-1362219 and DMR-1436006 (P.D.). This work is also supported by the Robert A. Welch Foundation Grant No. C-1839 (P.D.). Work performed by R.M.F. and J.K. is supported by the U.S. Department of Energy, Office of Science, Basic Energy Sciences, under Award No. DE-SC0012336.

[1] Y. Kamihara, T. Watanabe, M. Hirano, and H. Hosono, J. Am. Chem. Soc. **130**, 3296 (2008).

[2] C. de la Cruz, Q. Huang, J. W. Lynn, J. Li, W. Ratcliff II, J. L. Zarestky, H. A. Mook, G. F. Chen, J. L. Luo, N. L. Wang, and P. C. Dai, Nature (London) **453**, 899 (2008).

[3] D. C. Johnston, Adv. Phys. **59**, 803 (2010).

[4] P. C. Dai, Rev. Mod. Phys. **87**, 855 (2015).

[5] M. Rotter, M. Tegel, and D. Johrendt, Phys. Rev. Lett. **101**, 107006 (2008).

[6] S. Avci, O. Chmaissem, J. M. Allred, S. Rosenkranz, I. Eremin, A. V. Chubukov, D. E. Bugaris, D. Y. Chung, M. G. Kanatzidis, J.-P Castellan, J. A. Schlueter, H. Claus, D. D. Khalyavin, P. Manuel, A. Daoud-Aladine, and R. Osborn, Nat. Commun. **5**, 3845 (2014).

[7] F. Waßer, A. Schneidewind, Y. Sidis, S. Wurmehl, S. Aswartham, B. Büchner, and M. Braden, Phys. Rev. B **91**, 060505 (2015).

[8] J. M. Allred, K. M. Taddei, D. E. Bugaris, M. J. Krogstad, S. H. Lapidus, D. Y. Chung, H. Claus, M. G. Kanatzidis, D. E. Brown, J. Kang, R. M. Fernandes, I. Eremin, S. Rosenkranz, O. Chmaissem, and R. Osborn, Nat. Phys. **12**, 493 (2016).

[9] J. M. Allred, S. Avci, D. Y. Chung, H. Claus, D. D. Khalyavin, P. Manuel, K. M. Taddei, M. G. Kanatzidis, S. Rosenkranz, R. Osborn, and O. Chmaissem, Phys. Rev. B **92**, 094515 (2015).

[10] A. S. Sefat, R. Jin, M.A. McGuire, B. C. Sales, D. J. Singh, and D. Mandrus, Phys. Rev. Lett. **101**, 117004 (2008).

[11] L. J. Li, Y. K. Luo, Q. B. Wang, H. Chen, Z. Ren, Q. Tao, Y. K. Li, X. Lin, M. He, Z. W. Zhu, G. H. Cao, and Z. A. Xu, New J. Phys. **11**, 025008 (2009).

[12] D. K. Pratt, M. G. Kim, A. Kreyssig, Y. B. Lee, G. S. Tucker, A. Thaler, W. Tian, J. L. Zarestky, S. L. Bud'ko, P. C. Canfield, B. N. Harmon, A. I. Goldman, and R. J. McQueeney, Phys. Rev. Lett. **106**, 257001 (2011).

[13] X. Lu, H. Gretarsson, R. Zhang, X. Liu, H. Luo, W. Tian, M. Laver, Z. Yamani, Y.-J. Kim, A. H. Nevidomskyy, Q. Si, and P. Dai, Phys. Rev. Lett. **110**, 257001 (2013).

[14] A. D. Christianson *et al.*, Nature (London) **456**, 930 (2008).

[15] C. Zhang, M. Wang, H. Luo, M. Wang, M. Liu, J. Zhao, D. L. Abernathy, T. A. Maier, K. Marty, M. D. Lumsden, S. Chi, S. Chang, J. A. Rodriguez-Rivera, J. W. Lynn, T. Xiang, J. Hu, and P. Dai, Sci. Rep. **1**, 115 (2011).

[16] S. Chi, A. Schneidewind, J. Zhao, L. W. Harriger, L. Li, Y. Luo, G. Cao, Z. Xu, M. Loewenhaupt, J. Hu, and P. Dai, Phys. Rev. Lett. **102**, 107006 (2009).

[17] M. D. Lumsden, A. D. Christianson, D. Parshall, M. B. Stone, S. E. Nagler, G. J. MacDougall, H. A. Mook, K. Lokshin, T. Egami, D. L. Abernathy, E. A. Goremychkin, R. Osborn, M. A. McGuire, A. S. Sefat, R. Jin, B. C. Sales, and D. Mandrus, Phys. Rev. Lett. **102**, 107005 (2009).

[18] R. M. Fernandes and O. Vafek, Phys. Rev. B **90**, 214514 (2014).

[19] S. V. Borisenko, D. V. Evtushinsky, Z.-H. Liu, I. Morozov, R. Kappenberger, S. Wurmehl, B. Büchner, A. N. Yaresko, T. K. Kim, M. Hoesch, T. Wolf, and N. D. Zhigadlo, Nat. Phys. **12**, 311 (2016).

[20] J. H. Chu, J. G. Analytis, K. De Greve, P. L. McMahon, Z. Islam, Y. Yamamoto, and I. R. Fisher, Science **329**, 824 (2010).

[21] X. Y. Lu, K.-F. Tseng, T. Keller, W. L. Zhang, D. Hu, Y. Song, H. R. Man, J. T. Park, H. Q. Luo, S. L. Li, A. H. Nevidomskyy, and Pengcheng Dai, Phys. Rev. B **93**, 134519 (2016).

[22] J. J. Ying, X. F. Wang, T. Wu, Z. J. Xiang, R. H. Liu, Y. J. Yan, A. F. Wang, M. Zhang, G. J. Ye, P. Cheng, J. P. Hu, and X. H. Chen, Phys. Rev. Lett. **107**, 067001 (2011).

[23] E. C. Blomberg, M. A. Tanatar, R. M. Fernandes, I. I. Mazin, B. Shen, H.-H. Wen, M. D. Johannes, J. Schmalian, and R. Prozorov, Nat. Commun. **4**, 1914 (2013).

[24] R. M. Fernandes, A. V. Chubukov, and J. Schmalian, Nat. Phys. **10**, 97 (2014).

[25] H.-H. Kuo, J.-H. Chu, J. C. Palmstrom, S. A. Kivelson, and I. R. Fisher, Science **352**, 958 (2016).

[26] P. D. Johnson, H.-B. Yang, J. D. Rameau, G. D. Gu, Z.-H. Pan, T. Valla, M. Weinert, and A. V. Fedorov, Phys. Rev. Lett. **114**, 167001 (2015).

[27] Z. Li *et al.*, Phys. Rev. B **83**, 140506(R) (2011).

[28] M. H. Christensen, J. Kang, B. M. Andersen, I. Eremin, and R. M. Fernandes, Phys. Rev. B **92**, 214509 (2015).

[29] R. M. Moon, T. Riste, and W. C. Koehler, Phys. Rev. **181**, 920 (1969).

[30] Q. Huang, Y. Qiu, W. Bao, M. A. Green, J. W. Lynn, Y. C. Gasparovic, T. Wu, G. Wu, and X. H. Chen, Phys. Rev. Lett. **101**, 257003 (2008).

[31] S. L. Li, C. de la Cruz, Q. Huang, G. F. Chen, T.-L. Xia, J. L. Luo, N. L. Wang, and P. C. Dai, Phys. Rev. B **80**, 020504(R) (2009).

[32] N. Qureshi, P. Steffens, S. Wurmehl, S. Aswartham, B. Büchner, and M. Braden, Phys. Rev. B **86**, 060410 (2012).

[33] C. Wang, R. Zhang, F. Wang, H. Luo, L. P. Regnault, P. Dai, and Y. Li, Phys. Rev. X **3**, 041036 (2013).

[34] Y. Song, L.-P. Regnault, C. Zhang, G. Tan, S. V. Carr, S. Chi, A. D. Christianson, T. Xiang, and P. Dai, Phys. Rev. B **88**, 134512 (2013).

[35] O. J. Lipscombe, L. W. Harriger, P. G. Freeman, M. Enderle, C. Zhang, M. Wang, T. Egami, J. Hu, T. Xiang, M. R. Norman, and P. Dai, Phys. Rev. B **82**, 064515 (2010).
[36] H. Luo, M. Wang, C. Zhang, X. Lu, L.-P. Regnault, R. Zhang, S. Li, J. Hu, and P. Dai, Phys. Rev. Lett. **111**, 107006 (2013).
[37] P. Steffens, C. H. Lee, N. Qureshi, K. Kihou, A. Iyo, H. Eisaki, and M. Braden, Phys. Rev. Lett. **110**, 137001 (2013).
[38] C. Zhang, M. Liu, Y. Su, L.-P. Regnault, M. Wang, G. Tan, Th. Brückel, T. Egami, and P. Dai, Phys. Rev. B **87**, 081101 (2013).
[39] N. Qureshi, C. H. Lee, K. Kihou, K. Schmalzl, P. Steffens, and M. Braden, Phys. Rev. B **90**, 100502 (2014).
[40] C. Zhang, Y. Song, L.-P. Regnault, Y. Su, M. Enderle, J. Kulda, G. Tan, Z. C. Sims, T. Egami, Q. Si, and P. Dai, Phys. Rev. B **90**, 140502 (2014).
[41] M. Liu, C. Lester, J. Kulda, X. Lu, H. Luo, M. Wang, S. M. Hayden, and P. Dai, Phys. Rev. B **85**, 214516 (2012).
[42] Polarized neutron scattering results on $BaFe_2As_{1.4}P_{0.6}$.
[43] A. E. Bohmer, F. Hardy, L. Wang, T. Wolf, P. Schweiss, and C. Meingast, Nat. Commun. **6**, 7911 (2015).
[44] See Supplemental Material at http://link.aps.org/supplemental/10.1103/PhysRevB.94.214516 for additional data, details on data analysis, and details of the two band model.
[45] H. Man, X. Lu, J. S. Chen, R. Zhang, W. Zhang, H. Luo, J. Kulda, A. Ivanov, T. Keller, E. Morosan, Q. Si, and P. Dai, Phys. Rev. B **92**, 134521 (2015).
[46] J. T. Park, D. S. Inosov, A. Yaresko, S. Graser, D. L. Sun, Ph. Bourges, Y. Sidis, Y. Li, J.-H. Kim, D. Haug, A. Ivanov, K. Hradil, A. Schneidewind, P. Link, E. Faulhaber, I. Glavatskyy, C. T. Lin, B. Keimer, and V. Hinkov, Phys. Rev. B **82**, 134503 (2010).
[47] M. Wang, C. Zhang, X. Lu, G. Tan, H. Luo, Y. Song, M. Wang, X. Zhang, E. A. Goremychkin, T. G. Perring, T. A. Maier, Z. Yin, K. Haule, G. Kotliar, and P. Dai, Nat. Commun. **4**, 2874 (2013).
[48] A. Furrer, J. Mesot, and T. Strässle, *Neutron Scattering in Condensed Matter Physics* (World Scientific, Singapore, 2009).
[49] L. W. Harriger, H. Q. Luo, M. S. Liu, C. Frost, J. P. Hu, M. R. Norman, and P. Dai, Phys. Rev. B **84**, 054544 (2011).
[50] S. O. Diallo, D. K. Pratt, R. M. Fernandes, W. Tian, J. L. Zarestky, M. Lumsden, T. G. Perring, C. L. Broholm, N. Ni, S. L. Bud'ko, P. C. Canfield, H.-F. Li, D. Vaknin, A. Kreyssig, A. I. Goldman, and R. J. McQueeney, Phys. Rev. B **81**, 214407 (2010).
[51] M. M. Korshunov and I. Eremin, Phys. Rev. B **78**, 140509(R) (2008).
[52] S. Maiti, J. Knolle, I. Eremin, and A. V. Chubukov, Phys. Rev. B **84**, 144524 (2011).
[53] M. M. Korshunov, Y. N. Togushova, I. Eremin, and P. J. Hirschfeld, J. Supercond. Novel Magn. **26**, 2873 (2013).
[54] N. Qureshi, P. Steffens, D. Lamago, Y. Sidis, O. Sobolev, R. A. Ewings, L. Harnagea, S. Wurmehl, B. Büchner, and M. Braden, Phys. Rev. B **90**, 144503 (2014).
[55] P. Babkevich, B. Roessli, S. N. Gvasaliya, L.-P. Regnault, P. G. Freeman, E. Pomjakushina, K. Conder, and A. T. Boothroyd, Phys. Rev. B **83**, 180506 (2011).
[56] X. Lu, J. T. Park, R. Zhang, H. Luo, A. H. Nevidomskyy, Q. Si, and P. Dai, Science **345**, 657 (2014).
[57] Q. Zhang, R. M. Fernandes, J. Lamsal, J. Yan, S. Chi, G. S. Tucker, D. K. Pratt, J. W. Lynn, R. W. McCallum, P. C. Canfield, T. A. Lograsso, A. I. Goldman, D. Vaknin, and R. J. McQueeney, Phys. Rev. Lett. **114**, 057001 (2015).
[58] W. Zhang, J. T. Park, X. Lu, Y. Wei, X. Ma, L. Hao, P. Dai, Z. Y. Meng, Y.-f. Yang, H. Luo, and S. Li, Phys. Rev. Lett. **117**, 227003 (2016).